TECHNICAL REPORT R-78

ANALYTIC STUDY OF INDUCED PRESSURE ON LONG BODIES OF REVOLUTION WITH VARYING NOSE BLUNTNESS AT HYPERSONIC SPEEDS

By VERNON VAN HISE

Langley Research Center
Langley Field, Va.

TECHNICAL REPORT R–78

ANALYTIC STUDY OF INDUCED PRESSURE ON LONG BODIES OF REVOLUTION WITH VARYING NOSE BLUNTNESS AT HYPERSONIC SPEEDS

By VERNON VAN HISE

SUMMARY

A systematic study of induced pressures on a series of bodies of revolution with varying nose bluntness has been made by using the method of characteristics for a perfect gas. The fluid mediums investigated were air and helium and the Mach number range was from 5 to 40. A study of representative shock shapes was also made. Flow parameters obtained from the blast-wave analogy gave good correlations of induced pressures and shock shapes. The induced-pressure correlations yielded empirical equations for air and helium which cover the complete range of nose bluntness considered. (Nose fineness ratios varied from 0.4 to 4.) Available experimental results were in good agreement with the characteristics solutions. Properties connected with the concept of hypersonic similitude enabled correlations of the calculations to be made with respect to nose shape, Mach number, and ratio of specific heats.

INTRODUCTION

For very high Mach numbers, body surface pressures many times free-stream pressure can exist at large distances downstream from the nose of the body. The importance of knowing the magnitude of these blunt-nose induced pressures both from a loads standpoint and a heat-transfer standpoint has been established in reference 1. Also, induced pressures complicate the problem of measuring static pressure in hypersonic wind tunnels.

The present investigation presents pressure distributions determined by the method of characteristics for a series of nose shapes with long cylindrical afterbodies. The nose shapes considered are ogives, cones, pointed hemispheres, and Karman ogives; the noses have fineness ratios of from 0.4 to 4. Air and helium are the fluid mediums considered and are taken to be perfect gases in the calculations. Also included in the investigation is a study of some representative shock shapes. Comparisons of some available experimental data for both air and helium are made with the results of the present characteristic calculations.

The Mach number range of 5 to 40 along with the variety of nose shapes considered permits a study of some of the properties involved in the concept of hypersonic similitude. The present calculations are examined in the light of the similarities (see refs. 2 and 3, for example) that exist at very high Mach numbers.

SYMBOLS

d	diameter of cylindrical afterbody
n	nose-section fineness ratio, l/d
C_D	nose drag coefficient
K	hypersonic similarity parameter, M_∞/n
l	axial length of nose section (starting cone effect being disregarded; see fig. 1 for shapes A, B, and E)
M	Mach number
p	static pressure
p_σ	vertex pressure for true ogives (no starting cone)
R_d	Reynolds number based on diameter of cylindrical afterbody
x	distance along axis of symmetry
x_s	axial distance measured from junction of nose section and cylindrical afterbody (measured from shoulder)
y	distance along axis normal to x in the meridian plane (forms x,y coordinate system, see fig. 1)
y'	axis normal to x through vertex of starting cone
γ	ratio of specific heats

θ angle between local flow direction and x-axis

μ Mach angle relative to local flow direction, $\sin^{-1} 1/M$

σ semivertex angle of nose cone

Subscripts:

c nose-cone surface conditions

E refers to shape E

∞ free-stream conditions

BODY SHAPES

Figure 1 presents the body shapes for which flow fields were computed and shows the details of the six basic nose sections. For shapes A, B, and E a small tangent starting cone has been used to initiate the characteristics solution; this procedure changes the vertex location (y to y' in fig. 1) of the original nose shape a slight amount and also alters the flow properties which would occur for the original nose shape in the immediate area of the starting cone. The effect of these starting cones upon flow properties downstream of the starting cone should be relatively small; hence, if the original nose shape and its x,y axes are considered, all flow properties downstream of the starting cone are indicative of the flow properties of the original nose shape.

Shape C represents an effort to approximate a hemisphere-cylinder by attaching a nearly sonic cone in front of the hemisphere. The validity of this type of approximation has been established in reference 4 for the two-dimensional case. Shape E is a minimum drag nose shape (ref. 5) and is commonly referred to as the Karman ogive. Shape F has been designed by positioning a pointed hemisphere tangent to nose shape E at one-fourth its length. Table I presents a summary chart of the body shapes, Mach numbers, and ratio of specific heats for which flow fields were computed.

COMPUTATION PROCEDURE

The stepwise numerical calculation of the axisymmetric supersonic flow fields about the various body shapes was performed on the IBM 704 electronic data processing machine. The conical flow field at the front of each shape was computed by using the numerical technique of reference 6 for the case of the cone of revolution with axis parallel to the free stream. The remainder of the flow field was computed by applying the method of characteristics for axisymmetric rotational flow as outlined in reference 7. (Both rotational and irrotational calculations were made for body shape A.)

A preliminary investigation was undertaken to determine the characteristic net size and the number of approximations per net point which would give accurate surface pressures at large distances downstream from the nose. For the nose shapes and Mach number range of this paper the following general rules were found:

(1) The conical flow calculation should divide the angle between the cone surface and the cone shock into approximately 50 angular increments.

(2) For the corner expansion of shape D the characteristic lines emanating from the corner should be spaced at angular increments of approximately 2°. (At the corner between two consecutive characteristic rays, there should be a change in the sum $\theta+\mu$ of about 2°.)

(3) In the procedure for computing characteristic net points three approximations for each net point were necessary and consistent with the net fineness resulting from rules (1) and (2).

RESULTS AND DISCUSSION

CHARACTERISTIC SOLUTIONS FOR SURFACE PRESSURE

Figures 2 to 6 present the computed surface pressure distributions for all the combinations listed in table I. Figure 2 presents the pressures on shape A, the ogival nose with fineness ratio $n=4$, at Mach numbers to 40 in air with a comparison between the rotational and irrotational characteristic solution. It is seen that neglecting rotationality produces significant errors for this shape for Mach numbers about 5 and above, that is, when the hypersonic similarity parameter K exceeds unity. For blunter shapes significant errors could arise at Mach numbers considerably below 5. These curves of figure 2 represent an overlap and an extension of the range of the hypersonic similarity parameter given in references 8 and 9 and in this connection will be subsequently discussed in the section dealing with hypersonic similitude. Except for the irrotational solutions shown in figure 2, all other calculations are for the rotational case.

Figures 3 to 5 present a general picture of the effects of free-stream Mach number and ratio of specific heats upon surface pressure distributions.

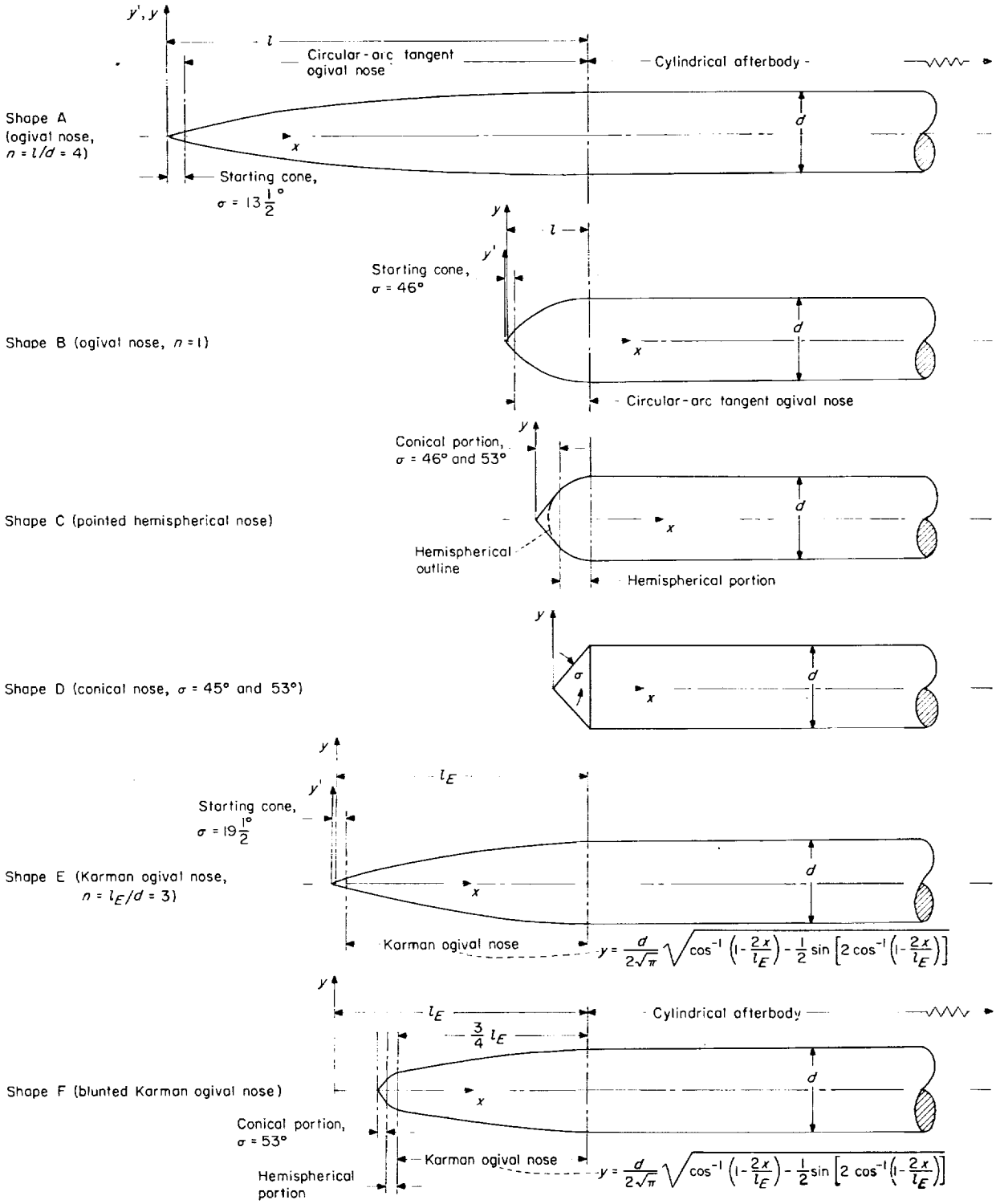

FIGURE 1.—Body shapes for which flow fields were computed.

TABLE I.—SUMMARY CHART OF VARIOUS COMBINATIONS COMPUTED

Nose shape	Condition	M_∞	γ	σ, deg	M_c	p_c/p_∞
Shape A (ogival nose, $n=4$)	1	2	7/5	13. 52	1. 76	1. 5
	2	3	7/5	13. 52	2. 58	1. 9
	3	4. 9	7/5	13. 52	3. 92	3. 2
	4	6. 9	7/5	13. 52	5. 03	5. 1
	5	10. 1	7/5	13. 52	6. 20	9. 4
	6	20	7/5	13. 52	7. 70	33
	7	40	7/5	13. 52	8. 29	129
Shape B (ogival nose, $n=1$)	1	5	7/5	46. 05	1. 41	20
	2	6. 9	7/5	46. 05	1. 56	38
	3	10	7/5	46. 05	1. 66	78
	4	20	7/5	46. 05	1. 73	310
	5	40	7/5	46. 05	1. 75	1, 227
	6	10	5/3	46. 05	1. 11	98
	7	20	5/3	46. 05	1. 16	387
Shape C (pointed hemispherical nose)	1	10	7/5	53. 2	1. 13	98
	2	20	7/5	53. 2	1. 19	387
	3	40	7/5	53. 2	1. 20	1, 537
	4	6. 9	7/5	46. 05	1. 56	38
	5	10	7/5	46. 05	1. 66	78
	6	18	7/5	46. 05	1. 73	248
	7	40	7/5	46. 05	1. 75	1, 227
	8	6. 9	5/3	46. 05	1. 06	48
	9	10	5/3	46. 05	1. 11	98
	10	18	5/3	46. 05	1. 15	314
	11	40	5/3	46. 05	1. 16	1, 540
Shape D (conical nose)	1	10	7/5	53. 1	1. 14	97
	2	20	7/5	53. 2	1. 19	387
	3	40	7/5	53. 2	1. 20	1, 537
	4	6. 9	7/5	45	1. 64	37
	5	10	7/5	45	1. 74	75
	6	19. 9	7/5	45	1. 82	295
	7	6. 9	5/3	45	1. 13	46
	8	10	5/3	45	1. 19	94
	9	17. 9	5/3	45	1. 23	298
Shape E (Karman nose, $n=3$)	1	6. 9	7/5	19. 55	4. 11	9. 1
	2	10	7/5	19. 55	4. 76	18
	3	20	7/5	19. 55	5. 43	67
Shape F (blunted Karman nose)	1	6. 9	7/5	52. 4	1. 11	47
	2	10	7/5	53. 2	1. 13	98
	3	20	7/5	53. 2	1. 19	387

For a given shape and ratio of specific heat, it is found that the pressure ratio p/p_∞ varies essentially as the square of the free-stream Mach number for surface regions influenced by a relatively strong bow shock. (The square-law variation has resulted since the pressure distributions of figures 3 to 5 include the hypersonic-flow regime in which the strong portion of the bow shock is essentially frozen.) For example, consider the top two curves in the left-hand part of figure 3. As the free-stream Mach number is varied from 20 to 40, it would be expected that the pressure ratio would rise fourfold. This is seen to hold true within 10 percent for x/d up to about 6. For the region

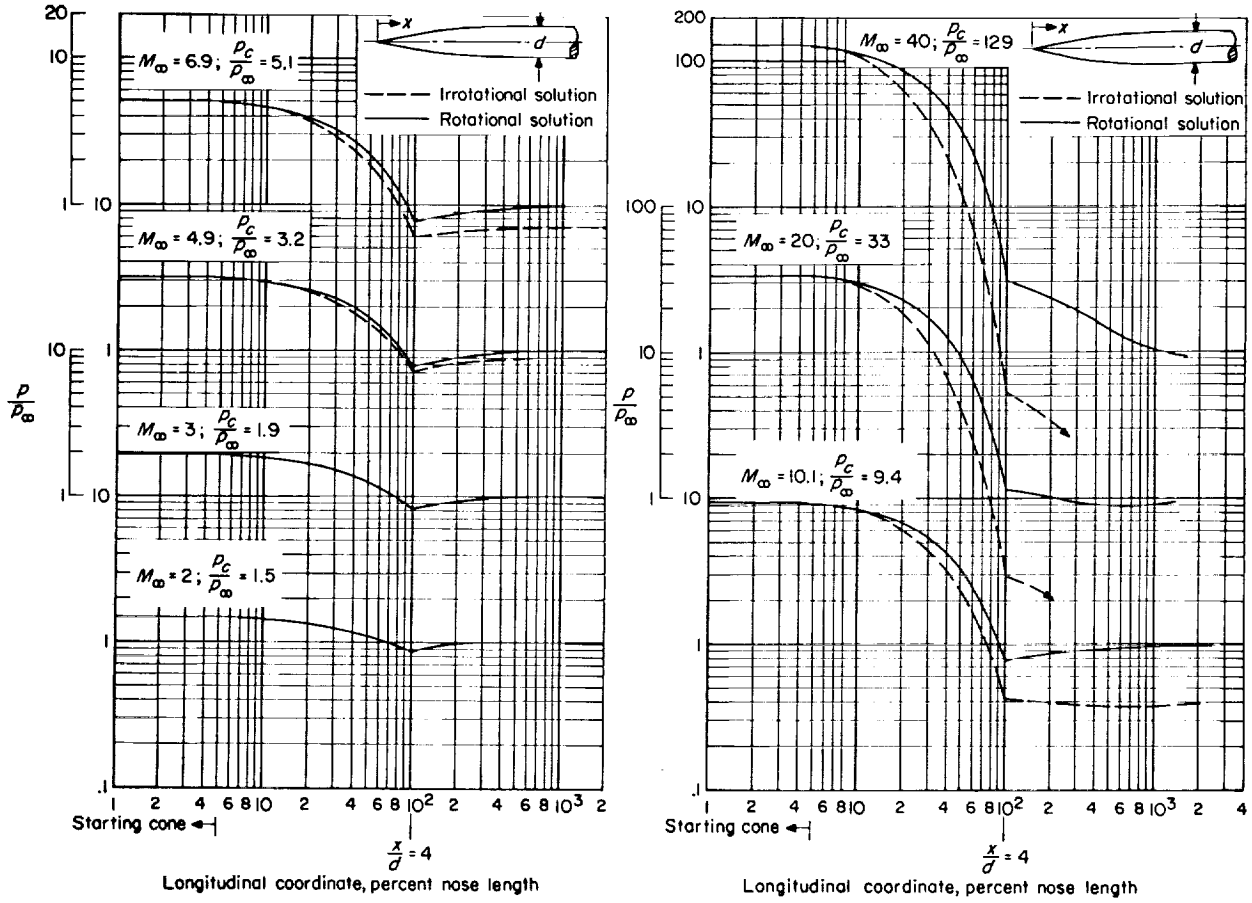

FIGURE 2.—Pressure distributions for shape A (ogival nose; $n=4$; $\gamma=7/5$) with comparison between the rotational and the irrotational solution.

with x/d greater than about 6, the square-law variation becomes less valid as would be anticipated since in this region the curve at a Mach number of 20 is influenced by a weak portion of the bow shock. Note that this square-law variation is equivalent to an invariance of pressure coefficient with free-stream Mach number.

An estimation of the effect of changing the fluid medium from air to helium can readily be ascertained from figures 3 to 5. For the cases shown in these figures it is found that, for the same nose shape and Mach number, the pressure level in helium is about 25 percent higher than in air except in the vicinity of the shoulder and for pressure ratios of about 1. Next compare the change from air to helium for combinations D–6 and D–9 in figure 5. In this case the Mach number has been changed so that the cone pressure ratios are essentially equal. Except for a small region just downstream of the shoulder, the two curves are about the same; hence, the effects of ratio of specific heat upon pressure distribution can be somewhat compensated for by an appropriate choice of Mach number.

Shape C (fig. 4) represents an approximation to a hemispherical nose which is suitable for calculations using the method of characteristics. The forward portion of the hemisphere is replaced by a cone with a half-apex angle such that the cone surface velocity is about sonic ($\sigma=53°$ for air and $\sigma=46°$ for helium). An indication as to the effects of this approximation is shown in figure 7. It is seen in the induced-pressure region for x/d greater than 3 that the change in vertex angle from $\sigma=46°$ to $\sigma=53°$ has resulted in a pressure change on the order of 5 percent. This change is in agreement with blast-wave theory (ref. 10) in which it is found that induced pressure varies as the square root of the nose drag coefficient.

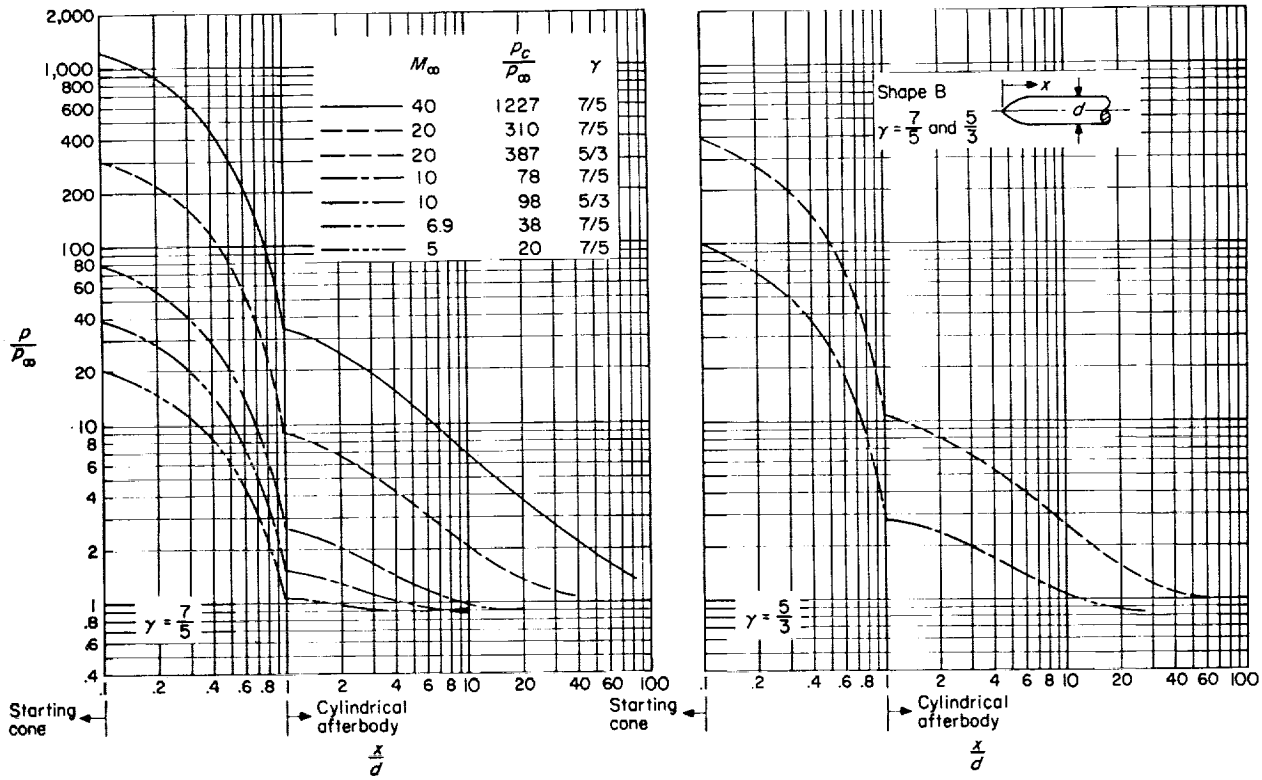

FIGURE 3.—Pressure distributions in air and helium for shape B (ogival nose; $n = 1$).

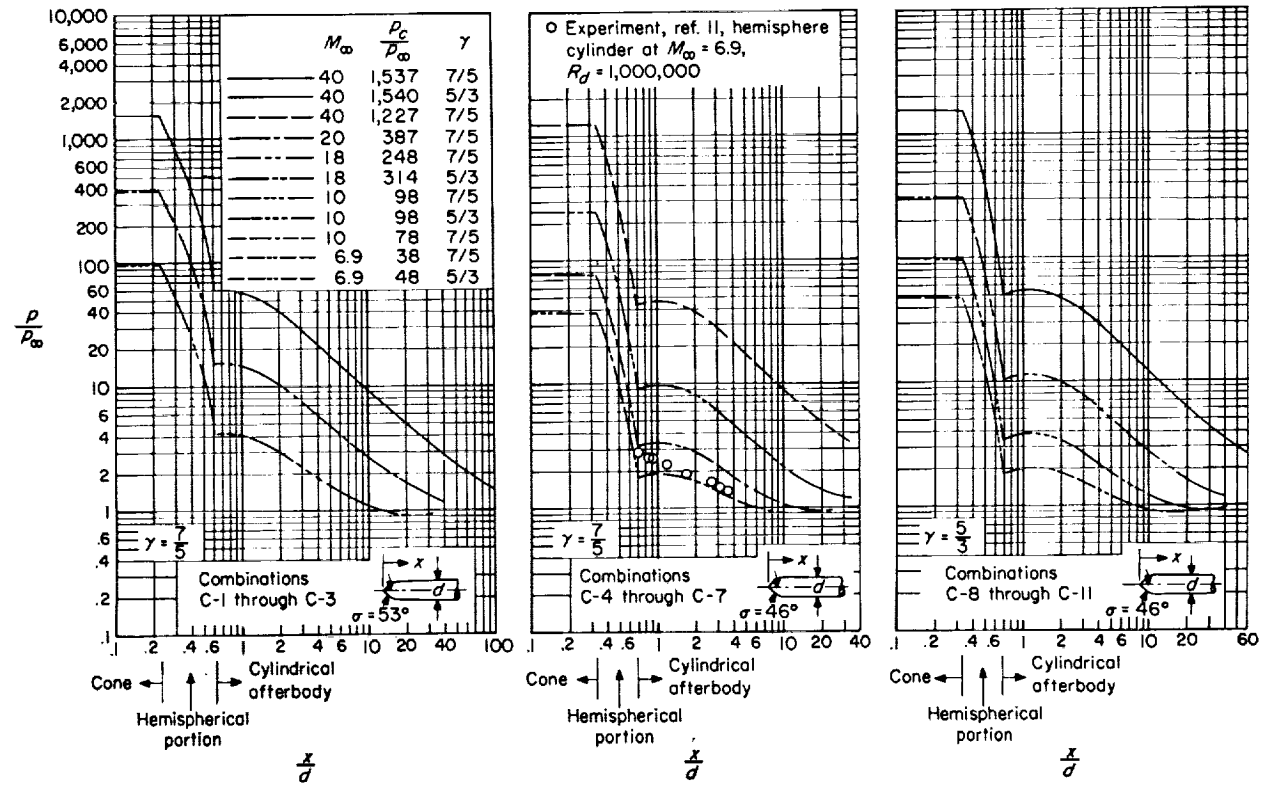

FIGURE 4.—Pressure distributions in air and helium for shape C (pointed-hemisphere nose).

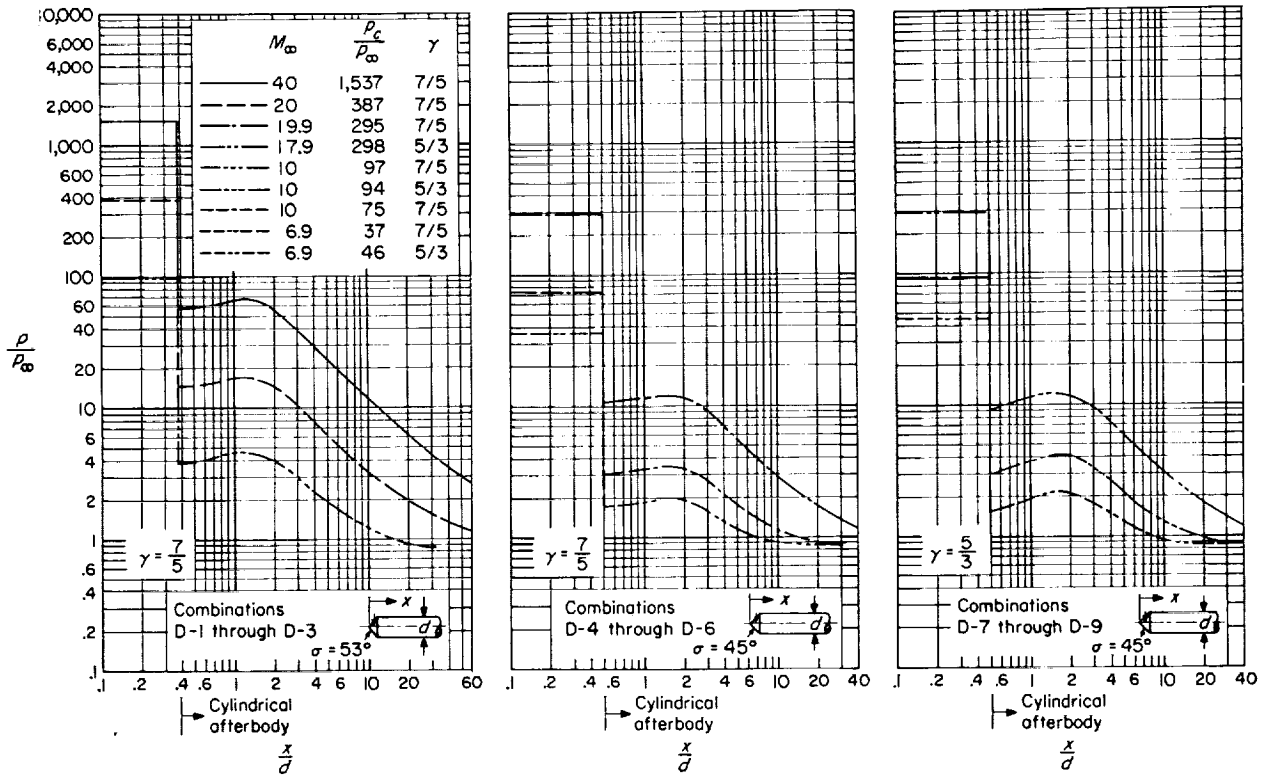

FIGURE 5.—Pressure distributions in air and helium for shape D (conical nose).

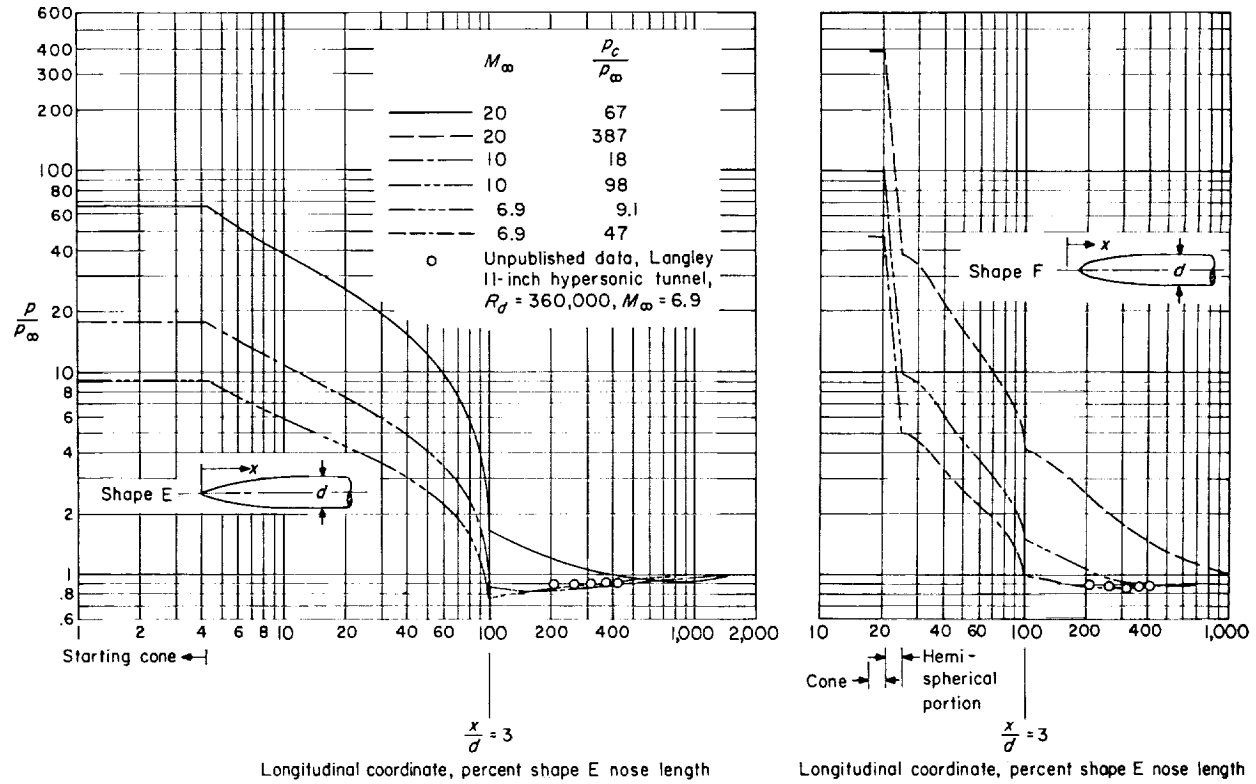

FIGURE 6.—Pressure distributions in air for shape E (Karman ogival nose; $n=3$) and shape F, its blunted counterpart.

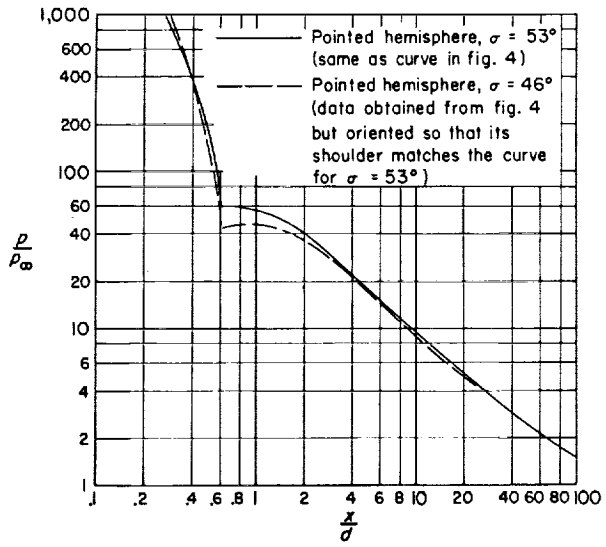

FIGURE 7.—Effect of vertex cone angle upon surface pressures of pointed hemisphere cylinders for air at a Mach number of 40.

Furthermore, blast-wave theory predicts only a 3-percent change in induced pressure between the pointed hemisphere cylinder ($\sigma=53°$) and a true hemisphere cylinder. Hence, for the case of air, the pointed hemisphere nose with $\sigma=53°$ is a good approximation to a true hemisphere nose for evaluating surface pressures for x/d greater than 3 and probably a fair approximation for most of the region upstream of $x/d=3$. Likewise for the case of helium, a consideration of nose drag coefficient shows that the pointed hemisphere nose with $\sigma=46°$ is a good approximation to a true hemisphere nose for determining surface pressures at x/d greater than 3.

In connection with the above discussion about shape C, figure 4 includes experimental pressures (ref. 11) for a hemisphere cylinder at a Mach number of 6.9. The shoulder of the hemisphere cylinder has been positioned at x/d equal to 0.70. For the station $x/d=3$, the difference between experiment (hemisphere nose) and characteristics theory (pointed hemisphere nose, $\sigma=46°$) is about that expected because of the difference in inviscid nose drag. Hence, for these pressure data it could be concluded that viscous effects upon surface pressure are relatively slight in the region of the cylindrical afterbody.

Figure 6 presents pressure distributions for shape E (the Karman ogival nose) and its blunted counterpart (shape F) for air at Mach numbers to 20. Blunting shape E has increased the pressure level at all Mach numbers as would be expected and the curves for a Mach number of 20 show that blunting has markedly increased the induced pressure on the cylindrical afterbody. Some unpublished pressure data obtained in the Langley 11-inch hypersonic tunnel at a Mach number of 6.9 are seen to be in agreement with the characteristic solutions shown in figure 6. Shape F, for which experimental results were obtained, has a hemisphere tangent to nose shape E at one-fourth its length. This is opposed to the pointed hemisphere of nose shape F for which computed results were obtained. Previously mentioned nose drag considerations show that the above-mentioned pressure data would be negligibly affected if the experimental shape F were the same as the computed shape F.

Figure 8 depicts the wide variation in pressure level induced by nose bluntness. The six basic nose shapes are shown for air at a Mach number of 20. Distances are measured from the shoulder. The high induced pressures which can occur on the cylindrical afterbody are the primary concern of this investigation.

BLAST-WAVE CORRELATION OF INDUCED PRESSURES

Reference 10 presents the cylindrical blast-wave solution and indicates its application in estimating the cylindrical afterbody pressures for the nose shapes of the present investigation. In accordance with this reference, it is found that the parameter

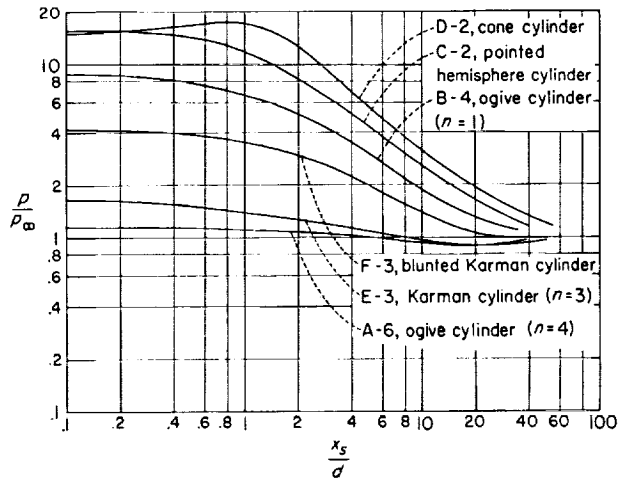

FIGURE 8.—Effect of nose bluntness on afterbody pressure level. $M_\infty=20$; $\gamma=7/5$.

governing the effect of nose bluntness upon induced pressure is $\frac{M_\infty^2 C_D^{1/2}}{x/d}$, where C_D is the nose drag coefficient. Figure 9 shows how this parameter correlates induced pressures over the entire range of nose bluntness considered, namely, from a fineness ratio of 0.4 to 4. Nose drag coefficients have been computed by using the nose pressure distributions given by the characteristic solutions in figures 2 to 6. For each of the combinations depicted, there is an x/d region extending downstream of the shoulder for which induced pressures have not been shown in figure 9. The induced pressures for these regions do not correlate according to the blast-wave analogy. Indeed, blast-wave theory does not deal with shoulder recompression regions such as found for the pointed hemisphere cylinders and the cone cylinders of figures 4 and 5. Reference 4 presents similar results for the shoulder regions in the two-dimensional case.

As seen in figure 9 the blast-wave pressure parameter correlates the induced pressures of this investigation into two distinct groups, one for air and one for helium. In accordance with the second-approximation form of the pressure equation which evolves from blast-wave theory, two equations have been fitted to these correlated characteristic results. These equations for air and helium, respectively, are:

$$\frac{p}{p_\infty}=0.060\,\frac{M_\infty^2 C_D^{1/2}}{x/d}+0.55 \qquad (1a)$$

$$\frac{p}{p_\infty}=0.075\,\frac{M_\infty^2 C_D^{1/2}}{x/d}+0.55 \qquad (1b)$$

These empirical equations do not account for induced pressures below free-stream pressure; however, these induced pressures do seem to correlate by using the blast-wave parameter. Equations (1a) and (1b) represent an empirical solution to the induced-pressure problem valid at least over the range of fineness ratio from 0.4 to 4.

Previously, it has been noted that, for the same nose shape and Mach number, the induced-pressure level in helium is about 25 percent higher

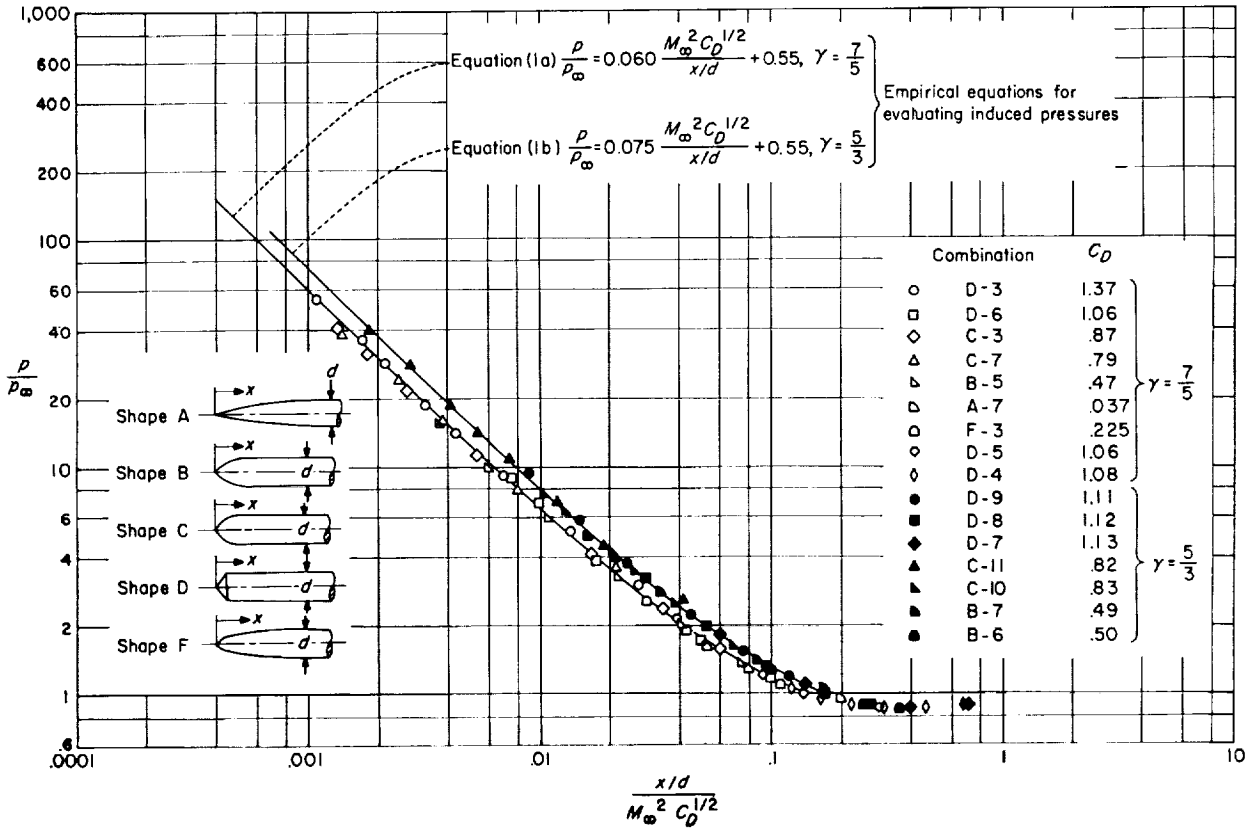

FIGURE 9.—Correlation of induced pressures by use of the cylindrical blast-wave pressure parameter.

than in air. (This value excluded the vicinity of the shoulder and pressures near free-stream pressure.) For any nose shape in this investigation, the variation in the square root of the nose drag coefficient between air and helium is at most a few percent. Hence, the ratio of the coefficients in equations (1a) and (1b), namely 0.075/0.060, should and does indicate the above-noted 25-percent change in pressure level.

In essence, equations (1a) and (1b) of figure 9 represent the blast-wave form of the method of characteristics; that is, except for a slight scatter in the correlated results of figure 9, good agreement is naturally expected between these equations and the characteristic solutions. Sample comparisons between the empirical equations (1a) and (1b) and the characteristic solutions are shown in figures 10 and 11 for air and helium, respectively. As previously discussed, these blast-wave theory curves deviate from the characteristic curves for a region extending downstream from the shoulder. An examination of the various comparisons depicted in figures 10 and 11 shows that agreement between the empirical blast-wave equations and the characteristic solutions begins at a distance about four nose lengths downstream of the shoulder.

Now that general equations for induced pressure (eqs. (1a) and (1b)) have been determined, a body such as a hemisphere cylinder can be considered on the basis of its nose drag. Figures 12 and 13 present a comparison of these equations with experimental data (refs. 12 and 13) obtained from hemisphere cylinders in air and helium. The nose

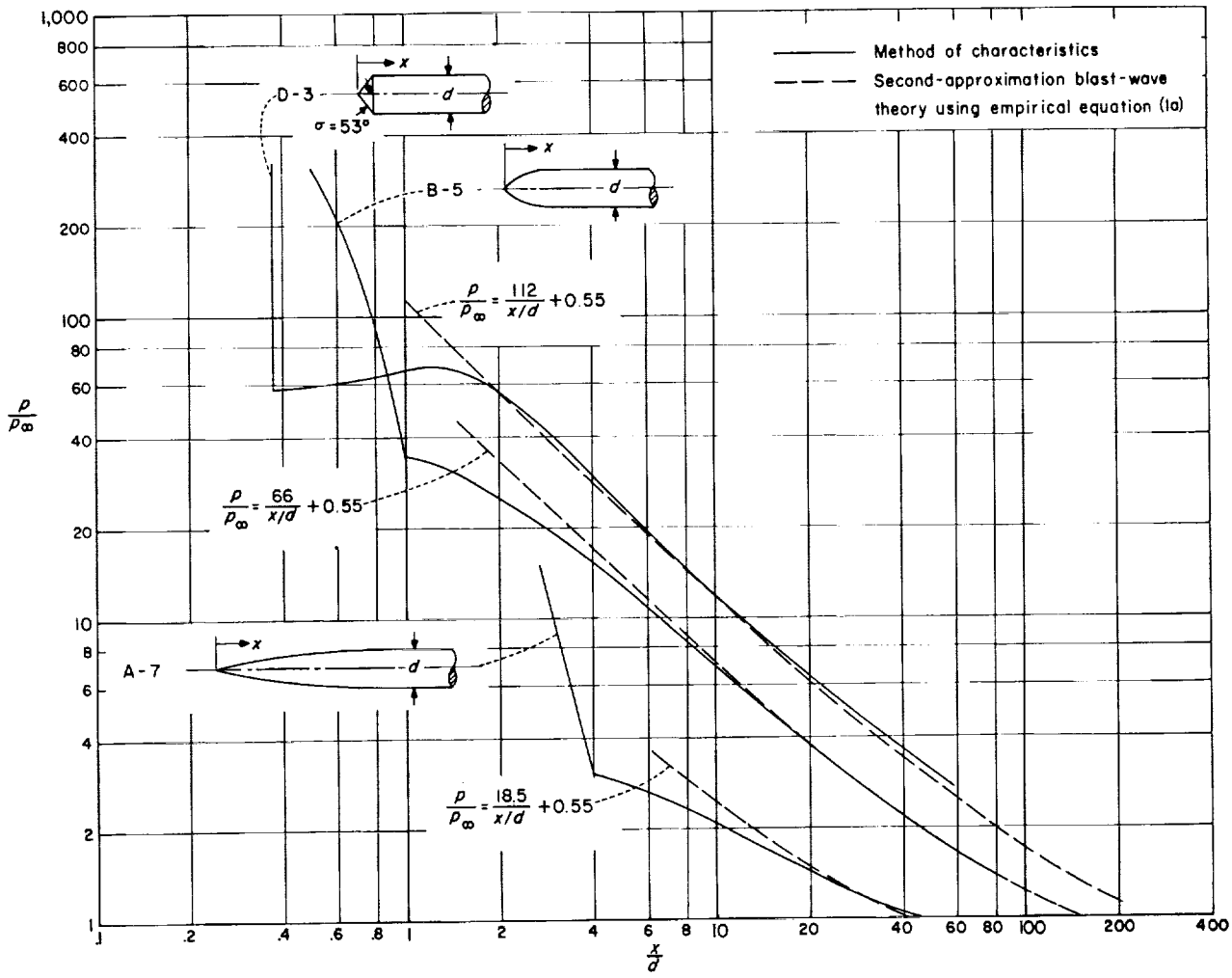

FIGURE 10.—Comparison of empirical equation (1a) with the characteristic solution. $M_\infty = 40$; $\gamma = 7/5$.

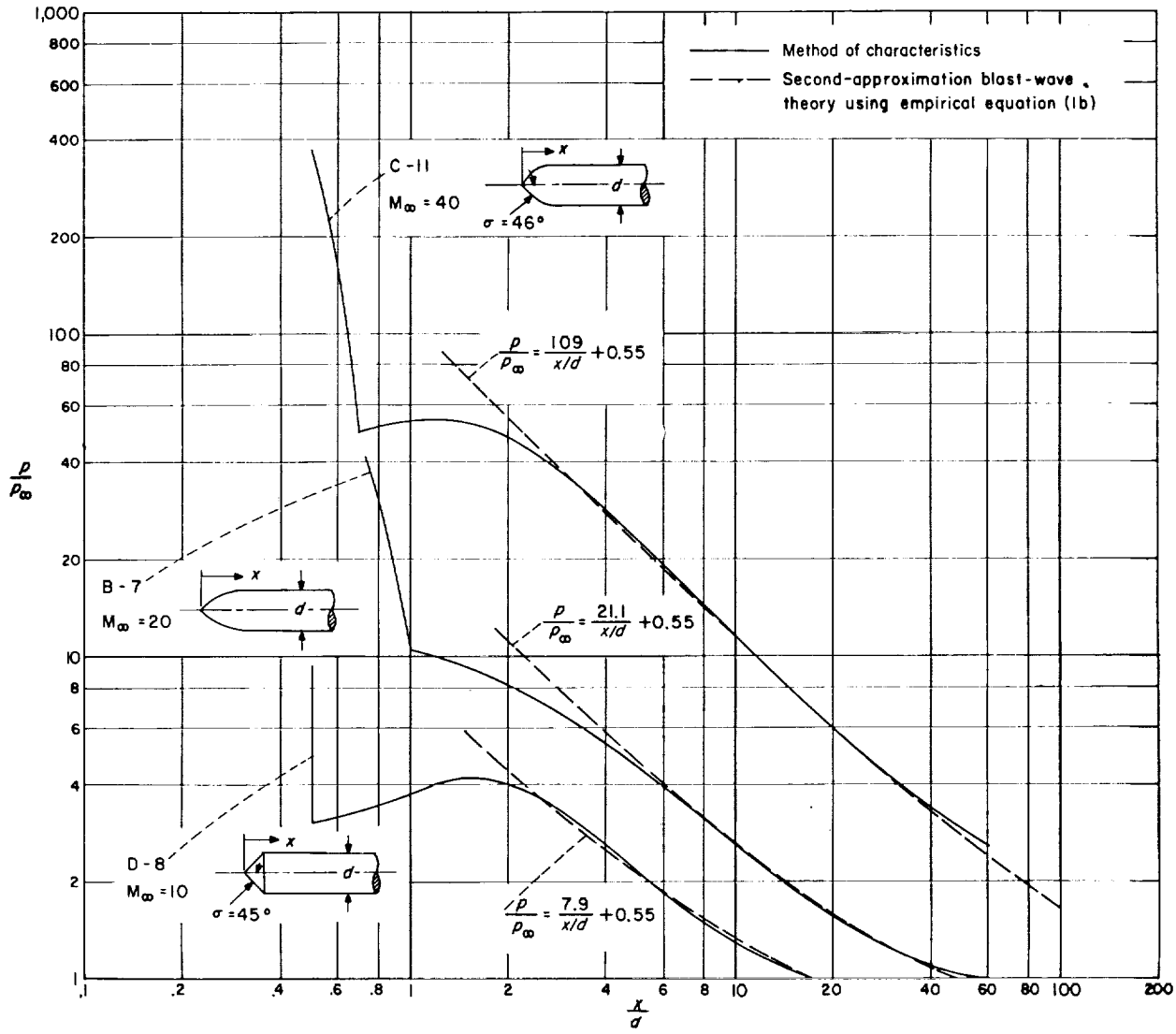

FIGURE 11.—Comparison of empirical equation (1b) with the characteristic solution. $\gamma = 5/3$.

drag coefficient for the hemisphere nose has been taken equal to the hypersonic approximation $\frac{1}{2}\left(\frac{\gamma+3}{\gamma+1}\right)$. The empirical equations of blast-wave theory are in agreement with the experimental induced pressures. (Reynolds numbers were 130,000 and greater.) As considered above, these equations are not expected to be valid upstream of an x/d value of about 2½ (equivalent to four nose lengths downstream from the shoulder) for the case of a hemisphere cylinder.

SHOCK-SHAPE STUDIES

The blast-wave parameter governing shock shape is $\frac{x}{d} C_D^{1/2}$. Figure 14 shows how this parameter correlates shock shapes over the range of nose bluntness in this investigation. Shock points for $\frac{x}{d} C_D^{1/2}$ less than about 1½ show considerable scatter on the log-log scale of this figure but really only represent a scatter on the order of $0.10\frac{y}{d}$.

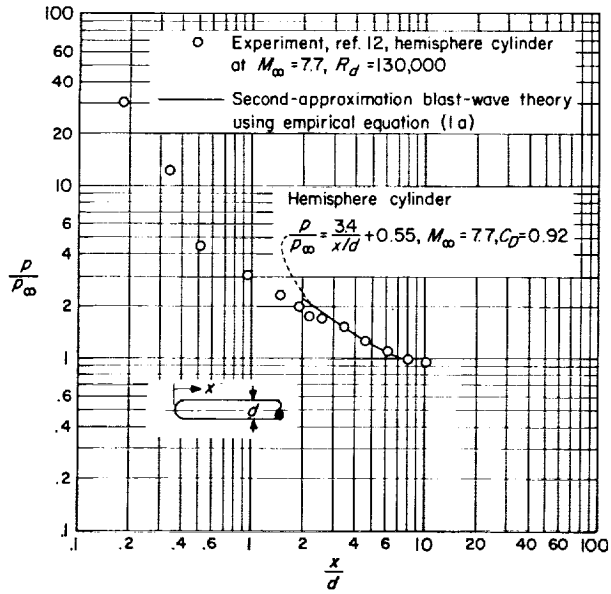

FIGURE 12.—Comparison of empirical equation (1a) with experiment. $\gamma = 7/5$.

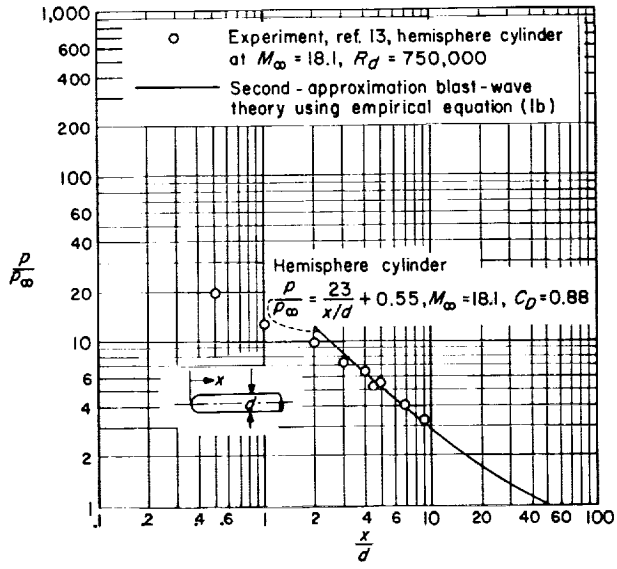

FIGURE 13.—Comparison of empirical equation (1b) with experiment. $\gamma = 5/3$.

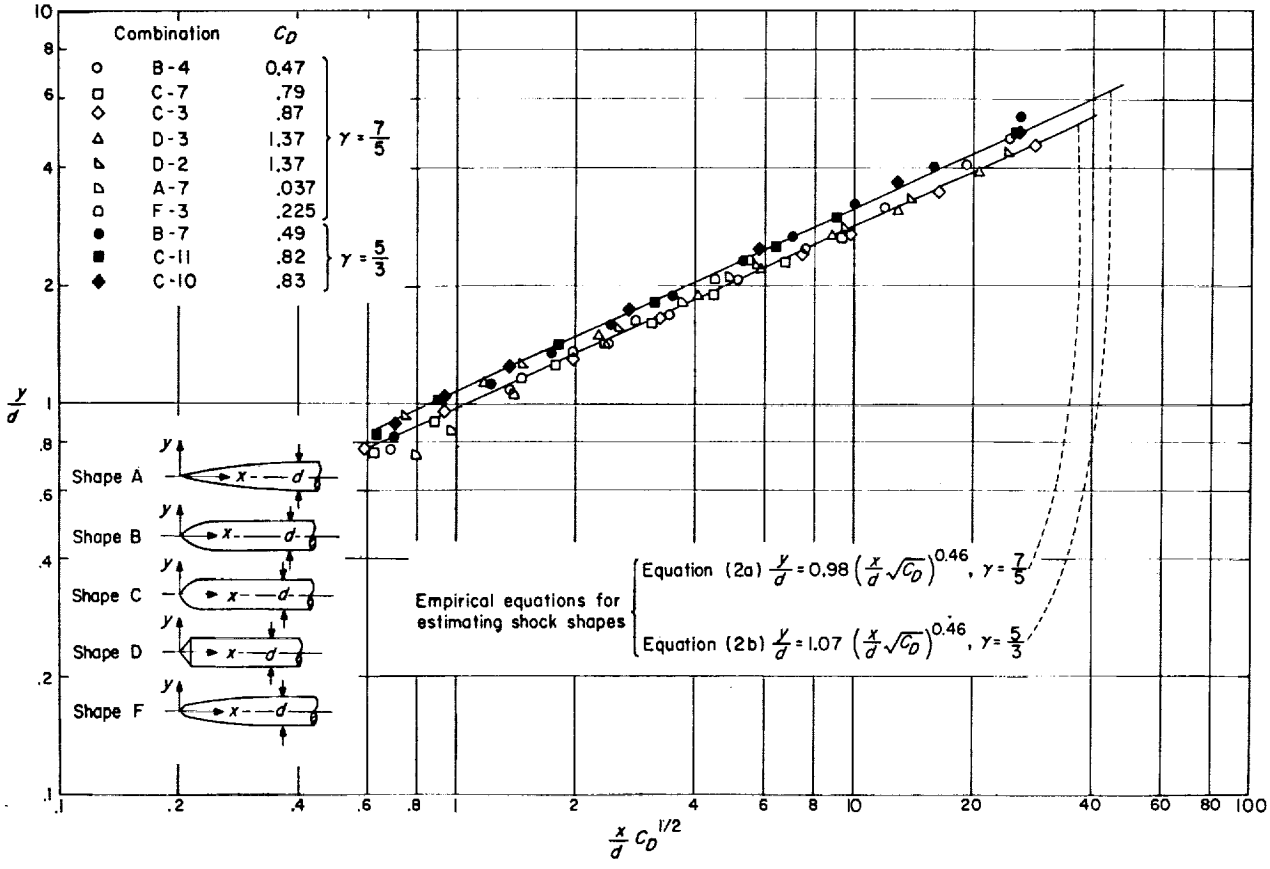

FIGURE 14.—Correlation of shock shapes by use of the cylindrical blast-wave shock-shape parameter.

Two straight lines have been faired through the two groups of points, one for air and one for helium. The equations of these lines for air and helium, respectively, are:

$$\frac{y}{d}=0.98\left(\frac{x}{d}\sqrt{C_D}\right)^{0.46} \tag{2a}$$

$$\frac{y}{d}=1.07\left(\frac{x}{d}\sqrt{C_D}\right)^{0.46} \tag{2b}$$

Equations (2a) and (2b) represent an empirical first-approximation blast-wave solution for shock shapes over the range of nose fineness ratio from 0.4 to 4.

The empirical power 0.46 (eqs. (2a) and (2b)) is somewhat less than ½ which is the theoretical power predicted by blast-wave theory. Since only a few shock shapes (fig. 14) were available for helium as opposed to air, the power in equation (2b) was kept at 0.46 as was found for equation (2a). However, these few helium shock shapes did indicate a tendency to yield an empirical power slightly higher than for air, say 0.47 or 0.48. This tendency is in agreement with findings in reference 14 where it is indicated that blast-wave theory should be more realistic for those gases with the larger specific heats.

Figure 15 presents a comparison of the empirical equations (2a) and (2b) with the characteristic solutions for the shock shapes of several combinations of nose shape, Mach number, and ratio of

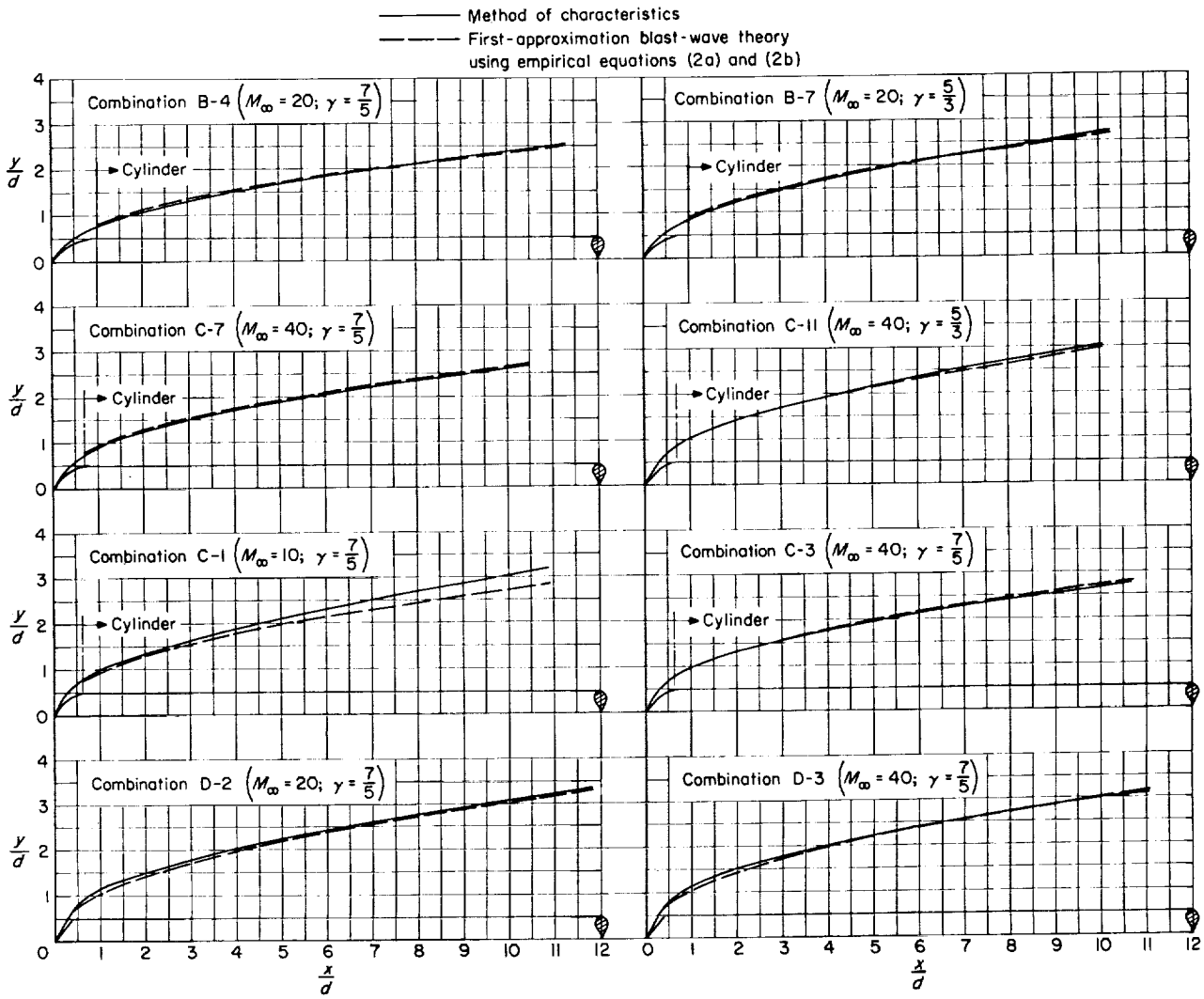

FIGURE 15.—Comparison of empirical equations (2a) and (2b) with the characteristic solution.

specific heats. Even though the correlation fairings (given by eqs. (2a) and (2b)) of figure 14 involve some scatter of shock points and represent only a first approximation, it is seen in figure 15 that equations (2a) and (2b) provide a good estimation of the characteristic solution except for combination C–1. This combination is for a free-stream Mach number of 10, and for Mach numbers this low a second-approximation blast-wave solution including Mach number effect is necessary to estimate shock shape.

The use of $\frac{x}{d} C_D^{1/2}$ as the shock-shape correlation parameter has neglected Mach number effects upon shock shape since the nose drag coefficient C_D is relatively insensitive to Mach number for Mach numbers greater than 5. Figure 16 shows the effect of Mach number upon shock shape. It is seen that shock-shape changes have become relatively slight for Mach numbers of about 20 or greater. A check of all the nose shapes ($n=4$ and less) of this investigation showed only small changes in shock shape above a Mach number of 20 for x_s/d up to about 10. (The flow field encompassed by the bow shock for these conditions is about 40 diameters of body length.) With regard to this discussion, all the combinations depicted in figure 14 are for Mach numbers of 20 or greater and yield correlation based upon the first-approximation blast-wave solution. Figure 17 indicates good agreement between empirical equation (2b) and experimental shock data for helium at a free-stream Mach number of 21.

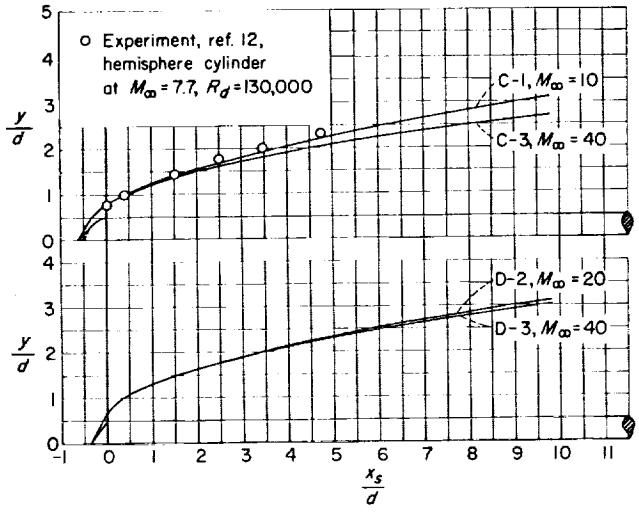

FIGURE 16.—Variation of shock shape with Mach number. $\gamma = 7/5$.

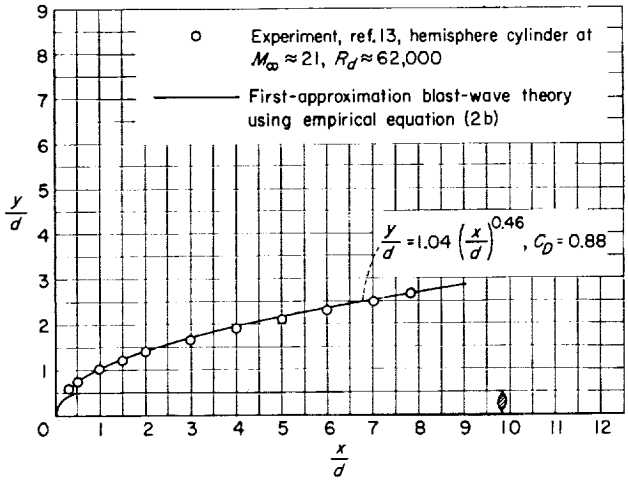

FIGURE 17.—Comparison of empirical equation (2b) with experiment. $\gamma = 5/3$.

HYPERSONIC SIMILITUDE AS EXEMPLIFIED BY THE CHARACTERISTIC CALCULATIONS

The results of reference 3 indicate that for very large free-stream Mach numbers the flow pattern and pressure coefficients on a given body become independent of free-stream Mach number. A fundamental property of this independence is that the density ratio across the bow shock be independent of the free-stream Mach number (often referred to as the strong shock condition). This property means that body bluntness will be a factor in determining the Mach number level at which independence of Mach number will occur.

The invariance of pressure coefficient with free-stream Mach number has been previously mentioned in the general discussion of figures 3 to 5. The shock-shape studies (in particular, fig. 16) have shown how the flow pattern at high Mach numbers has tended to become independent of Mach number. Indeed an examination of the characteristic nets for Mach numbers greater than about 20 showed that Mach line patterns also had become essentially independent of free-stream Mach number for about 40 diameters of body length. In regard to the concept of Mach number independence, it might be said that first-approximation blast-wave theory applies to this flow regime. Invariance of pressure coefficient is found in the first term of equations (1a) and (1b), whereas constancy of shock shape is apparent in equations (2a) and (2b).

References 2 and 15 propose a similarity law for

the rotational flow about slender bodies at hypersonic speeds. This law has correlated surface pressures for various families of bodies such as cone cylinders and ogive cylinders. (See refs. 8 and 9.) Figure 18 indicates the application of the hypersonic similarity law for the case of ogive cylinders with values of the hypersonic similiarity parameter K equal to 5 and 10. There is an expected difference between the pressure distributions of shapes A and B since reference 8 shows that nose fineness ratio should be greater than 2 for good correlation. However, although differences are present at the nose vertex, the agreement has become good on the cylindrical portion. Nose-vertex pressure differences at a given K become small for ogives with fineness ratios greater than 2. Hence indications are that for a given K (K on the order of 1 or greater) the pressure distributions of shape A are valid for any ogive cylinder with a nose section of fineness ratio greater than 2.

Reference 16 presents a generalized Newtonian theory that can be used as an aid in correlating pressure distributions for many of the cases in this investigation. When the concepts presented in this theory were considered, it was decided to reference surface pressure to maximum surface pressure in order to correlate the various nose-shape combinations. As will be seen in the discussion that follows, this type of correlation makes nose shape the main variable in determining pressure distribution and implies that the strong shock condition hold. (Note that the strong shock condition applies to blast-wave theory.)

Figure 19 shows good correlation of the pressure distributions for a group of ogival nose combinations. In this case pressures have been related to the vertex pressure of the true ogival shape of fineness ratio $n=1$ or $n=4$. Since the static pressure p has been assumed to be negligibly affected by the starting cones for 10 percent of the nose length and greater, the correlation distribution of this figure should cover true ogive cylinders of fineness ratio 1 or greater. However, the free-stream Mach number must be high enough that the strong shock condition holds; hence, each fineness ratio will have a minimum Mach number associated with it for this type of correlation.

Figure 20 shows that correlation on the basis of maximum surface pressure tends to eliminate the effects of ratio of specific heats as implied by the generalized Newtonian theory. This condition indicates that helium pressures will also correlate

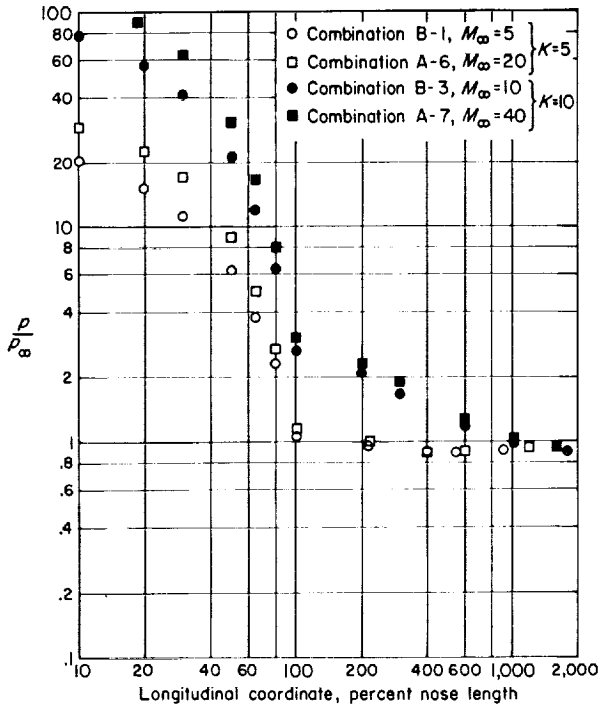

FIGURE 18.—Correlation of pressure distributions on ogive cylinders by use of the parameter K. $\gamma=7/5$.

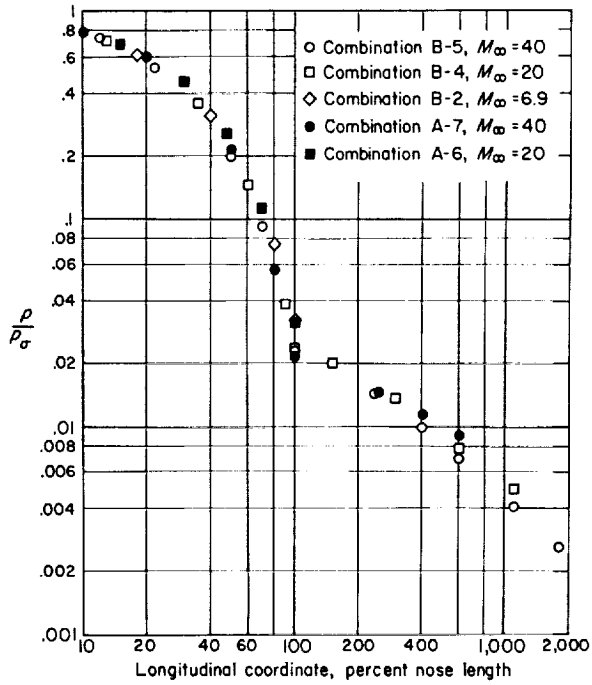

FIGURE 19.—Correlation of pressure distributions for several ogive-cylinder combinations. $\gamma=7/5$.

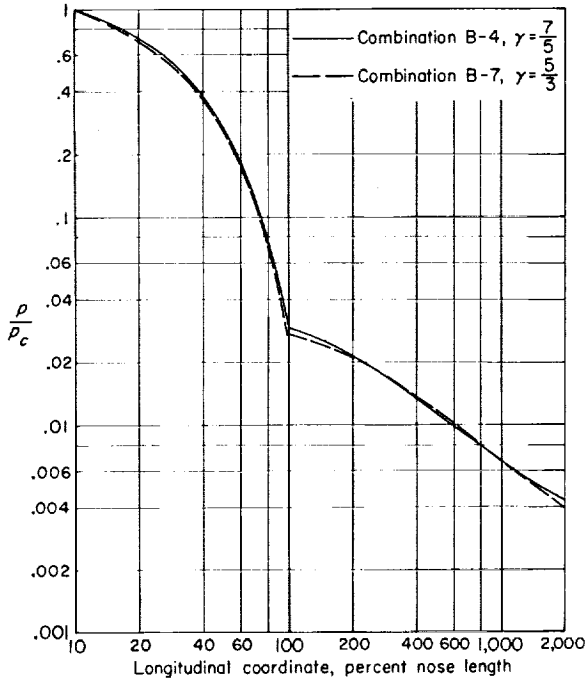

FIGURE 20.—Correlation of pressure distributions in air and helium for the ogive nose ($n=1$) at a Mach number of 20.

with the distribution of figure 19. This helium curve has not been included in figure 19 since the true ogive with a fineness ratio of 1 at a Mach number of 20 in helium gives a detached bow shock. In an application of generalized Newtonian theory to the case of ogives, reference 16 shows that p/p_σ on the surface of the ogive is a function only of the percent of the nose length and is independent of the fineness ratio. It is interesting to note in figure 19 that this functional relationship is still valid in the induced-pressure region.

An examination of equations (1a) and (1b), the empirical equations for evaluating induced pressures, indicated that, for the case of cone cylinders, nose fineness ratio does affect the ratio of induced pressure to cone pressure. Since the two cone shapes in this investigation had relatively small differences in fineness ratio, both shapes are presented in figure 21 for various Mach numbers and ratio of specific heats. Similarly, figure 22 presents the correlation of pressure distributions for several pointed hemisphere-cylinder combinations. Figures 21 and 22 show that, with the fineness ratio of the basic nose shape reasonably invariant, good correlation of induced pressures can be obtained by relating induced pressure to the maximum surface pressure. Pressure points on the order of free-stream pressure veer upward

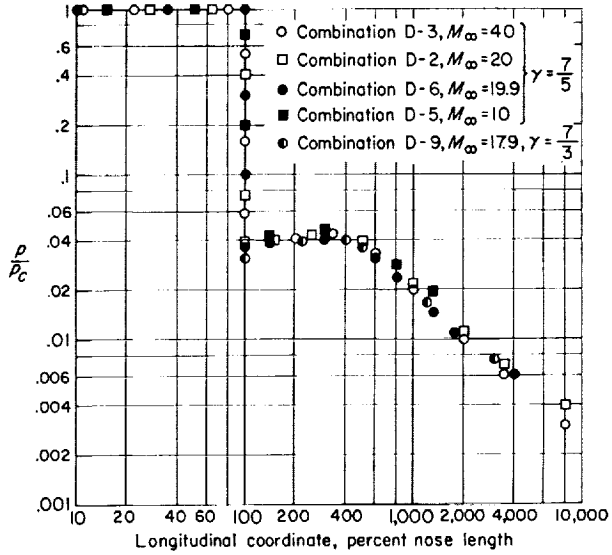

FIGURE 21.—Correlation of pressure distributions for several cone-cylinder combinations.

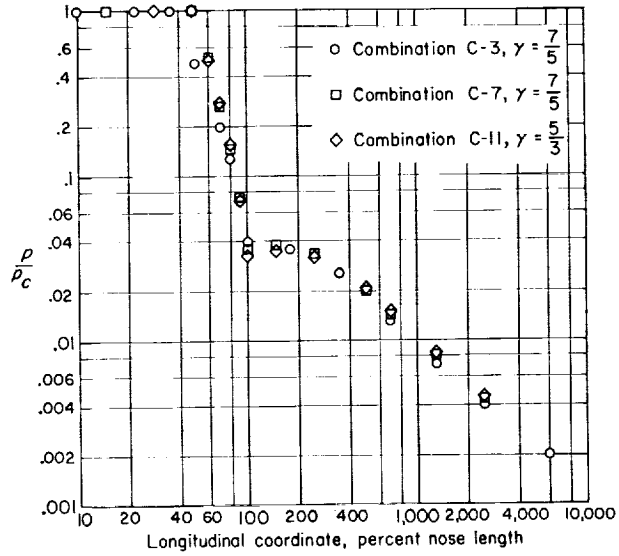

FIGURE 22.—Correlation of pressure distributions for a group of pointed hemisphere-cylinder combinations at a Mach number of 40.

from the main body of correlated points as illustrated by the end points of combination A–7 in figure 19 and combination D–5 in figure 21. These pressure points will not be expected to agree with this type of correlation, since their magnitudes are governed by relatively weak bow shock.

CONCLUSIONS

A systematic study using the method of characteristics has been made to determine the large induced pressures that can exist on a series of cylindrical afterbodies with varying nose bluntness. The Mach number range was from 5 to 40 and the fluid mediums, air and helium, were considered perfect gases throughout the calculations. Representative shock shapes were also investigated. This study yielded the following conclusions:

1. The blast-wave pressure parameter was found to correlate the induced pressures of the characteristic solutions throughout the range of fineness ratio considered, namely, fineness ratios from 0.4 to 4. The induced-pressure correlations yielded empirical equations for air and helium of the form given by the second-approximation blast-wave theory.

2. The blast-wave shock-shape parameter was found to correlate shock-shape solutions for Mach numbers of about 20 or greater. The shock-shape correlations yielded empirical equations of the form given by the first-approximation blast-wave theory.

3. The characteristic solutions (includes the empirical blast-wave equations derived from these solutions) and available experimental pressure and shock-shape data were in good agreement.

4. The hypersonic similarity law for slender bodies was found to correlate nose and afterbody pressures for ogive cylinders (with nose fineness ratios greater than 2) for values of the hypersonic similarity parameter K as high as 10.

5. For the strong shock condition, nose shape (ogives, hemispheres, cones, etc.) becomes a main variable in determining pressure distribution. The generalized Newtonian concept whereby surface pressure is referenced to maximum surface pressure was found to correlate not only nose pressures as is known but also induced pressures for ogive cylinders for various Mach numbers, fineness ratios, and fluid mediums. Also by referencing to maximum pressure the induced pressures for the two basic shapes, cone cylinders and pointed hemisphere cylinders, were found to correlate reasonably well for various Mach numbers and fluid mediums. (These two correlations are recognized as containing fineness-ratio effects.)

LANGLEY RESEARCH CENTER,
NATIONAL AERONAUTICS AND SPACE ADMINISTRATION,
LANGLEY FIELD, VA., *May 19, 1960.*

REFERENCES

1. Ferri, Antonio, and Pallone, Adrian: Note on the Flow Fields on the Rear Part of Blunt Bodies in Hypersonic Flow. WADC Tech. Note 56-294, U.S. Air Force, July 1956.
2. Tsien, Hsue-Shen: Similarity Laws of Hypersonic Flows. Jour. Math. and Phys., vol. XXV, no. 3, Oct. 1946, pp. 247–251.
3. Oswatitsch, Von Klaus: Ähnlichkeitsgesetze für Hyperschallströmung. Z.a.M.P., vol. II, fasc. 4, 1951, pp. 249–264.
4. Bertram, M. H., and Baradell, D. L.: A Note on the Sonic-Wedge Leading-Edge Approximation in Hypersonic Flow. Jour. Aero. Sci. (Readers' Forum), vol. 24, no. 8, Aug. 1957, pp. 627–629.
5. Von Kármán, Th.: The Problem of Resistance in Compressible Fluids. R. Accad. d'Italia, Cl. Sci. Fis., Mat. e Nat., vol. XIV, 1936, pp. 222–276. (Fifth Volta Congress held in Rome, Sept. 30–Oct. 6, 1935.)
6. Ferri, Antonio: Elements of Aerodynamics of Supersonic Flows. The Macmillan Co., 1949.
7. Ferri, Antonio: Application of the Method of Characteristics to Supersonic Rotational Flow. NACA Rep. 841, 1946. (Supersedes NACA TN 1135.)
8. Ehret, Dorris M., Rossow, Vernon J., and Stevens, Victor I.: An Analysis of the Applicability of the Hypersonic Similarity Law to the Study of Flow About Bodies of Revolution at Zero Angle of Attack. NACA TN 2250, 1950.
9. Rossow, Vernon J.: Applicability of the Hypersonic Similarity Rule to Pressure Distributions Which Include the Effects of Rotation for Bodies of Revolution at Zero Angle of Attack. NACA TN 2399, 1951.
10. Lin, Shao-Chi: Cylindrical Shock Waves Produced by Instantaneous Energy Release. Jour. Appl. Phys., vol. 25, no. 1, Jan. 1954, pp. 54–57.

11. Crawford, Davis H., and McCauley, William D.: Investigation of the Laminar Aerodynamic Heat-Transfer Characteristics of a Hemisphere-Cylinder in the Langley 11-Inch Hypersonic Tunnel at a Mach Number of 6.8. NACA Rep. 1323, 1957. (Supersedes NACA TN 3706.)
12. Lees, Lester, and Kubota, Toshi: Inviscid Hypersonic Flow Over Blunt-Nosed Slender Bodies. Jour. Aero. Sci., vol. 24, no. 3, Mar. 1957, pp. 195–202.
13. Mueller, James N., Close, William H., and Henderson, Arthur, Jr.: An Investigation of Induced-Pressure Phenomena on Axially Symmetric, Flow-Alined, Cylindrical Models Equipped With Different Nose Shapes at Free-Stream Mach Numbers From 15.6 to 21 in Helium. NASA TN D–373, 1960.
14. Hayes, Wallace D., and Probstein, Ronald F.: Hypersonic Flow Theory. Academic Press, Inc. (New York), 1959.
15. Hayes, Wallace D.: On Hypersonic Similitude. Quarterly Appl. Math., vol. V, no. 1, Apr. 1947, pp. 105–106.
16. Love, E. S.: Generalized-Newtonian Theory. Jour. Aero/Space Sci. (Readers' Forum), vol. 26, no. 5, May 1959, pp. 314–315.

U.S. GOVERNMENT PRINTING OFFICE: 1961